MDPI

Article

Coupled Geophysical and Hydrogeochemical Characterization of a Coastal Aquifer as Tool for a More Efficient Management (Torredembarra, Spain)

Alex Sendrós [1,2,*], Ingrid J. Cubides [3], Mahjoub Himi [1], Raúl Lovera [1,2], Aritz Urruela [1], Josefina C. Tapias [2,4], Lluís Rivero [1,2], Ruben Garcia-Artigas [5] and Albert Casas [1,2]

1   Department of Mineralogy, Petrology and Applied Geology, Universitat de Barcelona, 08028 Barcelona, Spain; himi@ub.edu (M.H.); rlovera@ub.edu (R.L.); aritz.urruela@ub.edu (A.U.); lrivero@ub.edu (L.R.); albert.casas@ub.edu (A.C.)
2   Water Research Institute, Universitat de Barcelona, 08001 Barcelona, Spain; jtapias@ub.edu
3   School of Geology, Industrial University of Santander, Bucaramanga 680003, Colombia; ingridcubides65@gmail.com
4   Department of Biology, Health and Environment, Universitat de Barcelona, 08028 Barcelona, Spain
5   Agència Catalana de l'Aigua, Generalitat de Catalunya, 08008 Barcelona, Spain; ruben.garciaa@gencat.cat
*   Correspondence: alex.sendros@ub.edu

Abstract: The aquifers of the Spanish Mediterranean coast are generally subjected to intense exploitation to meet the growing water supply demands. The result of the exploitation is salinization due to the marine saltwater intrusion, causing a deterioration in the quality of the water pumped, limiting its use for community needs, and not always being well delimited. To prevent deterioration, a groundwater control network usually allows precise knowledge of the areas affected by saltwater intrusion but not the extent of the saline plumes. Moreover, the characterization of aquifer systems requires a model that defines the geometry of aquifer formations. For this objective, we integrated hydrogeological, hydrogeochemical, and electrical resistivity subsoil data to establish a hydrogeological model of the coastal aquifer of Torredembarra (Tarragona, NE Spain). In this research, we have carried out a regional and local-scale study of the aquifer system to define the areas prone to being affected by saline intrusion (electrical resistivity values below 10 $\Omega \cdot m$). The obtained results could be used as a support tool for the assessment of the most favorable areas for groundwater withdrawal, as well as enabling the control and protection of the most susceptible areas to be affected by saltwater intrusion.

Keywords: aquifer geometry; electrical resistivity tomography; saltwater intrusion; geoelectrical sounding; groundwater sustainability

1. Introduction

Surface water resources in coastal areas are often scarce, and the aquifers play a pivotal role in managing the complex issue of water supply [1–3]. Aquifers are an underground set of rock or sediment formations that are saturated and permeable enough to transmit economical amounts of water to springs and wells, generating for all living beings a greater possibility of access to a drinkable water resource [4]. Aquifers also have a primordial relationship with the wetlands and ecosystems present around them, greatly influencing the genesis and preservation of these waters, which is why they are of significant use for survival, especially for human beings [5].

However, the accelerated increase in economic and demographic development in worldwide coastal areas in general, and in Spain in particular, has generated a natural imbalance [6,7]. The increasing water demand, because of per capita demand and population increases, causes a strongly increasing exploitation of the available high-quality water resources, increasing the risk of salinization via the mixing of fresh and saltwater

and generating marine intrusion [8]. Marine intrusion is a dynamic process in which saltwater from the sea moves inland during periods of lower aquifer recharge and recedes towards the aquifer when freshwater recharge from the continent increases, resulting in the mixing of these waters and the contamination of the aquifers that supply the need for water resources [9,10].

These trends can be further worsened in large areas by the enduring effects of climate change [11]. All of these conditions are causing stress on water resources, especially in terms of the risks of groundwater quality degradation in the case of coastal aquifers [12]. Over the decades, all of the described increasing difficulties, including environmental concerns, have highlighted the need to improve the management of groundwater resources [13–15].

Spain is a country that is mostly surrounded by continental and island coasts, and it is there where most of its population is located, as well as a series of aquifers of vital interest due to the volume and strategic nature of the water resources they store [16].

The aquifers of the Spanish and Catalan Mediterranean coast are generally subjected to intense exploitation to meet the growing water supply needs for domestic, tourist, industrial, and agricultural uses [17]. The result of the intense exploitation, mainly by sustained groundwater pumping, is salinization due to the marine saltwater intrusion, causing a deterioration in the quality of the water pumped and limiting its use for certain needs of the community [18].

To prevent the quality deterioration of groundwater resources, the Catalan Water Agency (ACA) has designed a piezometric network for monitoring salinity and the groundwater decline and depletion caused by intensive pumping. The network has 190 groundwater control points, and conductivity, pH, and temperature are analyzed in situ, as are the concentrations of the majority of anions and cations in the laboratory. The monitoring system allows precise knowledge of the zones affected by saltwater intrusion but not the extent of the saline plumes [19].

The use of wells and piezometers that have already been drilled and equipped, as well as the use of lithological logs, aquifer water sampling, and water table measurements, are all examples of direct hydrogeological procedures classically used. The logs and hydrochemical data only provide punctual information on the water quality, hydraulic data, and aquifer geometry. Additionally, a model that specifies the geometry and structural boundaries of aquifer formations is necessary for the hydrogeological and hydrogeochemical characterization of aquifer systems [20].

Indirect methods, such as near-surface geophysical techniques, have been extensively used in groundwater research in coastal locations to acquire this key information. Geophysical techniques are high-resolution methods that reveal details about the physical characteristics of the subsoil and its spatial distribution on a variety of working scales [21,22]. Moreover, the large electrical resistivity contrast between seawater (0.2 Ωm) and freshwater (>5 Ω·m) makes it possible to map the subsurface groundwater salinity distribution using geoelectrical techniques [23]. When lithological data are scarce or unable to provide the detailed subsurface knowledge needed for groundwater modeling, these non-invasive techniques become beneficial. Vertical electrical soundings (VES) [24–27] and Electrical resistivity tomography (ERT) are geoelectrical methods widely used to characterize coastal aquifer characteristics and properties such as on the Morocco coastal rift [24], Southwest Portugal [28], Pucket (Thailand) coastal aquifer [25], and delineating seawater intrusion on Monterrey (Mexico) [29], Bela Plain (Pakistan) [30], and also in Mediterranean coastal aquifers such as Cap-Bon (Tunisia) [31], South-Western Sicily (Italy) [32], River Nil Delta (Egypt) [33,34]; Rhodope (Greece) [35], Port de la Selva (Spain) [36] and Vélez Málaga (Spain) [37] among others.

The procedure used in this research combines the acquisition of new geophysical data with the use of publicly available geophysical data from the Spanish Geological and Mining Survey (IGME) and hydrochemical data from the Water Catalan Agency (ACA), and we consider it to have three fundamental advantages for developing new assessment tools: speed of application, resolution, and an efficient cost-benefit ratio.

We have conducted a regional-scale qualitative and quantitative study of the aquifer system to define a hydrogeological conceptualization of the coastal aquifer, to characterize the hydrogeochemistry of groundwater, and to identify the areas prone to being affected by the saline intrusion. The results could be utilized as a decision-supporting tool to evaluate the most favorable locations for groundwater extraction as well as control the most susceptible zones to be affected by saltwater intrusion. In addition, the use of indirect geophysical methods will limit the number of new piezometers and the subsequent risk of coming into contact with different aquifer units during drilling operations.

2. Study Area

The studied zone is situated northeast of the Iberian Peninsula and southeast of the Camp de Tarragona basin. The area is limited to the north by the Bonastre Massif and to the south by the Mediterranean Sea (Figure 1).
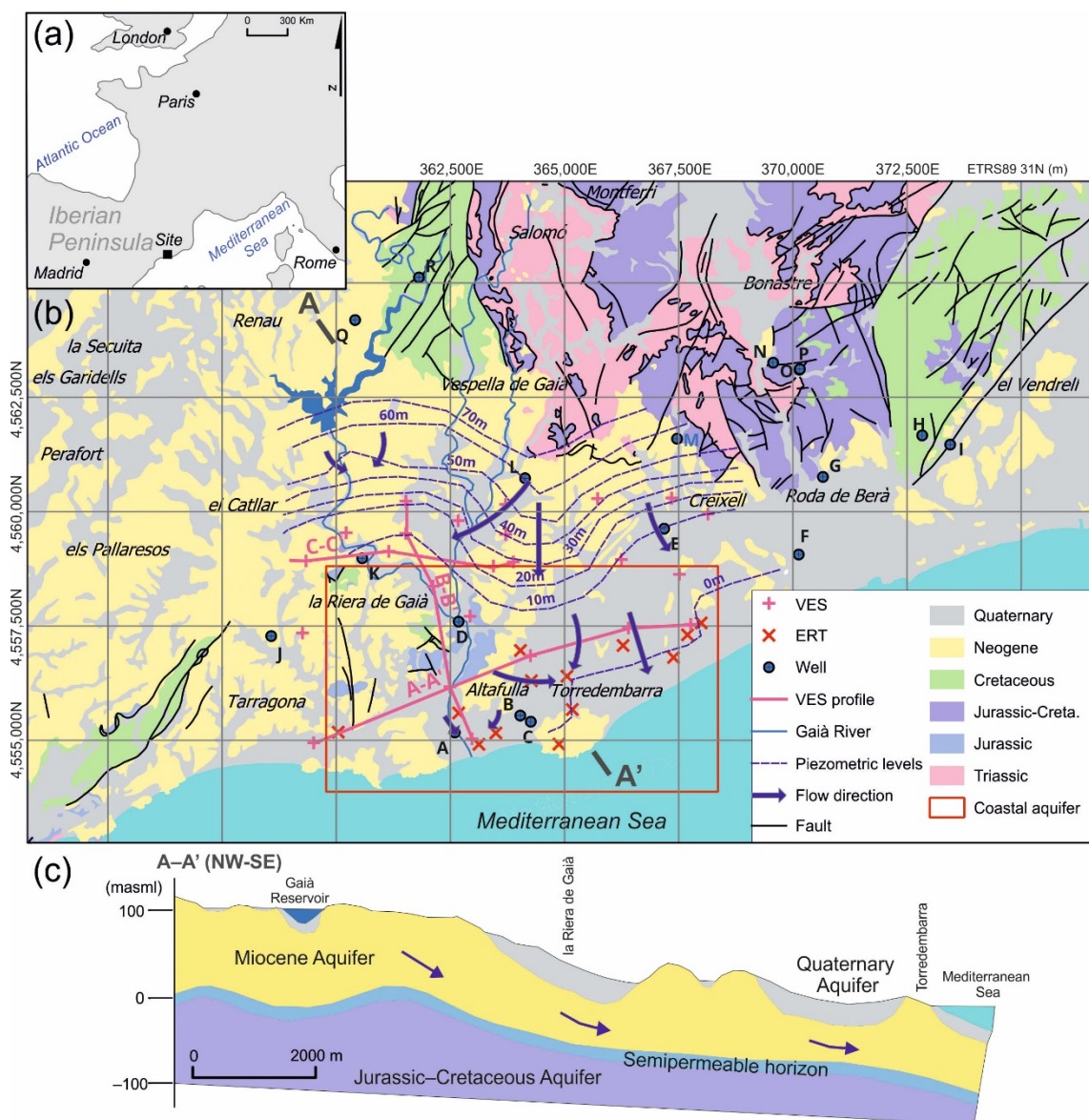
Figure 1. (**a**) Location sketch of the site; (**b**) Hydrogeological setting of the Catllar-Torredembarra site and geophysical (Vertical Electrical Sounding-VES and Electrical Resistivity-ERT) and hydrogeochemical (well) data used for the present research. Piezometric surfaces are in meters above mean sea level. Modified from [38,39]; (**c**) hydrogeological cross-section. Modified from [40].

The region has a Mediterranean climate with a warm thermal regime in the summer (average of 26 °C in July) and a moderately cold thermal regime in the winter (average of 8 °C in February). The yearly rainfall ranges, on average, from 550 to 650 mm/year. The wettest months are reported in the autumn, whereas July is the driest month and has the highest potential evapotranspiration values [41].

Surface water resources are consequently scarce. The Gaià River is the main resource, having an average discharge rate of 0.3 m^3/s (2015–2020) [42], and its 60.5 hm^3 reservoir is used for petrochemical industrial and agriculture supply [43].

The municipalities of the studied area use groundwater for water supply, similar to other Mediterranean coastal regions, and have undergone extensive urbanization along with a concomitant shift away from an agricultural and fishing economy to one governed by the expansion of tourism from the 1960s to the present. Due to the surge in water use for recreational purposes and tourists, particularly during the summer, the area's water demands have therefore significantly increased, when the Torredembarra and Altafulla populations reach 475,000 inhabitants compared to 21,000 inhabitants during the winter or non-tourist season [44].

The Camp de Tarragona zone is the result of the sedimentary filling of an Oligocene tectonic trench between the Pre-Coastal and Coastal Catalan mountain ranges [45]. It is filled by sediments from the Miocene to the Quaternary of marine or continental origin due to denudation of the southern edge of the Pre-Coastal Mountain Range [46]. This arrangement forms a multilayer system in which, basically, there are two hydrogeological units with different potentials but which coexist with other deep aquifers with independent hydrogeological functioning subject to a hydraulic connection in favor of fractures in deep calcareous levels.

The Quaternary and Miocene aquifers would form the same hydrogeological unit in this study area since they are hydraulically connected; this would therefore be the most important aquiferous unit in the area in terms of exploitation and outcrop extension. The Quaternary aquifer is formed by Plio-Quaternary gravels of fluvial-torrential and piedmont origin in hydraulic contact with conglomerates, continental sandstones, and Miocene calcarenites in the sector of the Francolí River (located west of the studied zone). The shallow aquifer has a free aquifer behavior with an average thickness of 10–15 m and high transmissivity values of up to 2.3–3.5 × 10^{-2} m^2/s, where clastic sediments dominate, favoring its intense exploitation [47]. The underground flow is perpendicular to the Mediterranean, except in the Francolí alluvial, whose bed drains laterally to the aquifer.

The Miocene Aquifer, on the other hand, has multilayer behavior. The average thickness of the Miocene infills is 50 to 300 m, and transmissivities are variable from medium to high, with values of 5 to 20 × 10^{-4} m^2/s [47]. The piezometric surface ranges from 110 m above mean sea level to the north of the Gaià Reservoir and less than 1 m above sea level on the coast, which in the Torredembarra areas even reaches below sea level [39].

The lower aquifer is called the Jurassic-Cretaceous Aquifer, which is made up of two hydraulically interconnected formations: basal Miocene conglomeratic breccias and Mesozoic calcareous-dolomitic materials, located at an average depth of 100–140 m, with minimum depths of 250–300 m depending on the tectonic effect. Its permeability is very high, of a secondary-fractured type, with which transmissivities are also high, up to 20 × 10^{-4} m^2/s.

The elevation of the piezometric surface ranges between 2 and 200 m above sea level; the greatest gradients are around Bonastre Massif, becoming smoother towards the western sector and the coastline of the unit, maintaining an N-S flow except in the recharge zone, where there is a small divergence that distributes the flow towards the southwest and towards El Vendrell.

In general terms and according to the authors of [40], recharge totals 41.6 hm^3/year, basically from the infiltration of rainfall and contributions from other lateral units, infiltration from rivers and reservoirs, or the return of irrigation. The most important discharge is towards the sea, with a flow of 17.8 hm^3/year, although a flow of 20 hm^3/year between

the Gaià Cretaceous block and the neighboring sub-units and pumping of 6.3 hm^3/year must be taken into account.

3. Materials and Methods

3.1. Groundwater Quality Assessment

Hydrochemical characterization of this study area was carried out using groundwater physicochemical parameters from the database of the Water Catalan Agency control network [42]. We have selected hydrochemical data from the 18 control groundwater points that are available in this study area. The control points are water wells and piezometers from 6 to 450 m deep with an average of 100 m depth and are used for monitoring three different water bodies defined in 2002 to fulfill the Water Framework Directive (Directive 2000/60/EC) (Table 1).

Table 1. The Catalan Water Agency controlled the control network of the studied site during the period 2105–2020 [42]. Water type classification is based on major ion content.

Id	Water Body	Well Depth (m)	Number of Samples	Water Type
A	Lower Gaià	12	6	chloride-calcium (2015–2017)/calcium-bicarbonate (2020)
B	Garraf	13	2	chloride-sodic
C	Lower Gaià	6	1	chloride-sodic
D	Garraf	120	2	calcium-bicarbonate
E	Lower Gaià	100	4	magnesium-bicarbonate
F	Lower Gaià	31	3	magnesium-bicarbonate
G	Lower Gaià	118	6	calcium-bicarbonate
H	Not defined	10	4	calcium-bicarbonate
I	Garraf	100	2	calcium-bicarbonate
J	Lower Gaià	80	6	chloride-sodic
K	Lower Gaià	158	3	magnesium-bicarbonate
L	Lower Gaià	100	6	calcium-bicarbonate
M	Not defined	180	4	calcium-bicarbonate
N	Not defined	118	6	calcium-bicarbonate
O	Gaià-Bonastre Massif	120	2	calcium-bicarbonate
P	Not defined	140	4	calcium-bicarbonate
Q	Gaià-Bonastre Massif	450	5	calcium-bicarbonate
R	Not defined	64	6	calcium-bicarbonate

The water samples were collected and transported by the own staff of ACA to their laboratory following a quality assurance management system [48]. For the analysis of the inorganic elements, the ACA laboratory uses an inductively coupled plasma mass spectrometry instrument) and follows the criteria and specifications of the international standards [49].

The parameters that are commonly analyzed in all of them (pH, temperature, electrical conductivity (EC), Ca^{2+}, Na^{2+}, Mg^{2+}, K^+, HCO_3^-, Cl^-, SO_4^{2-}, and NO_3^+). and periodic monitoring were selected for the present research. The network is monitored twice a year: in the dry seasons between June and August (Summer) when the water demand is considerably high, and in September and November (Autumn) when the demand has decreased and they are preparing for the winter. Both summer and autumn data were evaluated over the last five years with complete and available data (from 2015 to 2020) (Table 1).

The quality and representativeness of the analytical results have been assessed by calculating the percentage error for all chemical analyses, considering only the data provided for major ions.

$$error(\% = 100\frac{\sum cations - \sum anions}{\sum cations + \sum anions}$$

We have obtained, as a result, a relative error of ionic balance between 0.75% and 3.87% with a mean of 2.3%, which we consider an admitted value and in accordance with the geological and environmental conditions present at this study site.

The hydrogeochemical data were sorted and plotted out using the software EASYQUIM v5.0 [50], which generates the main chemical diagrams such as Piper [51], Schöeller-Berkaloff [52], and Stiff [53] for further analysis and interpretation.

3.2. Geoelectrical Surveys

In this research, we have used Vertical Electrical Soundings (VES) data acquired in the 1980s for the Spanish Mining and Geological Survey (IGME) and Electrical Resistivity Tomography (ERT) data acquired in 2021. Electrical surveys generally have the scope of identifying the subsurface resistivity distribution through surface measurements. The true resistivity of the subsoil can be calculated from these observations. In unconsolidated sediments, the porosity—presuming all pores are water-saturated—and clay concentration both affect electrical resistivity (typically, sandy soil has a higher resistivity than clayey soil). Nevertheless, there is an overlap in the values for different types of soils and rocks due to the fact that the resistivity of a particular soil or rock sample depends on several properties, including porosity, the degree of water saturation, and the concentration of dissolved salts [54].

The ERT is a geophysical method that is regarded as the contemporary development of traditional geoelectrical techniques such as VES [26] and electrical trenching. The basic basis is the same; however, in this technique, computer-controlled multi-electrodes that change automatically are employed in place of the conventional four electrodes fixed in the soil surface with a common basic spacing (two for energizing and two for monitoring the voltage generated) [55].

The larger number of electrodes arranged on a line and the larger volumes of soil in which properties and boundaries can be identified in space and time have made ERT surveys less labor-intensive and more cost-effective than previous VES campaigns [56]. The current is injected into the ground through electrodes 1 and 4 in the simplest geometry (that of a Wenner array), and the potential difference between electrodes 2 and 4 is measured. The apparent resistivity value gathered is attributed to being below the midpoint of the four electrodes. A trapezium of measurements is created by choosing various electrode combinations and employing multiples of the base electrode spacing. Typically, this is represented as a pseudosection in which the vertical axis is related to the survey length.

Measurements were made in this research using the Syscal Pro multi-electrode system (IRIS instruments, Orléans, France). Multielectrode systems generate a significant amount of data, necessitating automated data management and processing. There are three steps involved in working with the resistivity data. The first is creating a pseudosection, which is an initial approximation of a picture created by plotting each acquired apparent resistivity value. The second is the removal of geometrical effects from the mathematical inversion processing, which transforms the observed data into a picture of genuine depths and true formation resistivities. The geological interpretation of the resulting physical parameters is the last phase.

The VES survey apparent resistivity data from IGME were inverted in IPI2WIN software v3.0.1 [57], allowing for the obtaining of the 1D geoelectric response of the subsoil.

The apparent resistivity values of the ERT data were inverted using the RES2DINV program v3.54.44 [58]. This software uses a non-linear optimization technique via least-squares fitting to divide the subsurface into cells with specified dimensions, for which the resistivities are changed iteratively until a satisfactory agreement between the input

data and the model responses is reached [59]. The root mean square (RMS) value of the difference between experimental data and the revised model response is used as a criterion to gauge convergence at each iteration step throughout the inversion process. The inversion is considered to converge, and the procedure is finished if the data error RMS value, or the relative decrease of the data error RMS value, falls below a pre-defined level.

4. Results and Discussion

4.1. Groundwater Quality Assessment

Seventy-three water samples with physicochemical parameters and major ionic concentration results were available in the Water Catalan Agency database (18 control points and the 2015–2020 period). The ionic content of the samples ranged from medium to high (EC between 559 and 3043 µS/cm) (Table 2). Based on the concentrations provided in the European Water Directive (Directive 98/83/EC), which coincides with the limits laid down by Spanish legislation (R.D. 140/2003), 25% of the water samples could not be directly used for drinking water purposes. The main water issues, according to the Directive and major ion concentration, are related to chloride concentration (14% of the samples > 250 mg/L), nitrate concentration (9% of the samples are above 50 mg/L), and sulfate concentration (8% of the samples > 250 mg/L).

Table 2. Descriptive statistics for the physical-chemical parameters of the control groundwater network (2015–2020 period). The number of samples considered is 73.

|	T	pH	EC	Na^+	K^+	Cl^-	HCO_3^-	SO_4^{2-}	NO_3^-	Ca^+	Mg^{2+}
	°C		µS/cm	mg/L	mg/L	mg/L	mg/L	mg/L	mg/L	mg/L	mg/L
Min	13.7	6.7	599	12.3	1.0	21.6	162.0	54.5	4.9	36.7	31.8
Max	23.5	8.3	3043	431.0	10.0	610.1	385.8	292.5	170.8	168.0	99.0
Mean	19.5	7.5	1298	83.5	4.1	147.5	326.6	145.4	36.54	97.3	54.3
SD	2.5	0.3	658	109.3	2.6	172.1	50.4	74.0	40.5	29.0	18.1

Nitrate concentrations had the most widespread impact and were probably the most difficult to solve in the region of Catalonia (northeast of Spain). This is essentially a result of fertilization practices, particularly the application of livestock manure [60].

Chloride concentrations are usually used as salinity indicators and could increase as a result of over-pumping [61], especially in coastal areas due to the effect of marine intrusion [62].

For the analysis of the marine intrusion, a series of ionic ratio plots have been carried out to evidence the presence of ionic relations and to characterize the presence of marine intrusion in the sector:

- As can be identified in Figure 2a, a clear linear relationship (Coefficient of Determination R^2 = 0.9015) is identified where the increase in EC is directly related to the increase in chloride concentration. Since the chloride ion is a conservative ion and there are no geological units in the sector that could contribute this ion to the water, its origin, and concentration are related to anthropogenic origin and/or marine intrusion events.
- The samples located upstream of the Riera de Gaià show lower concentrations of Na and Cl with respect to the more coastal waters (Figure 2b). However, it is important to mention that most of the samples are aligned, with a value of the ratio between these ions close to 0.85, a value of 0.85 corresponding to seawater composition.
- The majority of the water samples have a rCl/rHCO₃ ratio between 0.1 and 5; therefore, their characteristics are more like those of inland waters (Figure 2c). Nevertheless, the ratio is increasing at points close to the shoreline, indicating a slight marine influence [54].

- From Figure 2d, it can be seen that the samples tend to have a ratio of 0.1, which indicates the value of the seawater ratio; however, there is a degree of dispersion in the samples, probably associated with the wide origin of the sulfate [63].
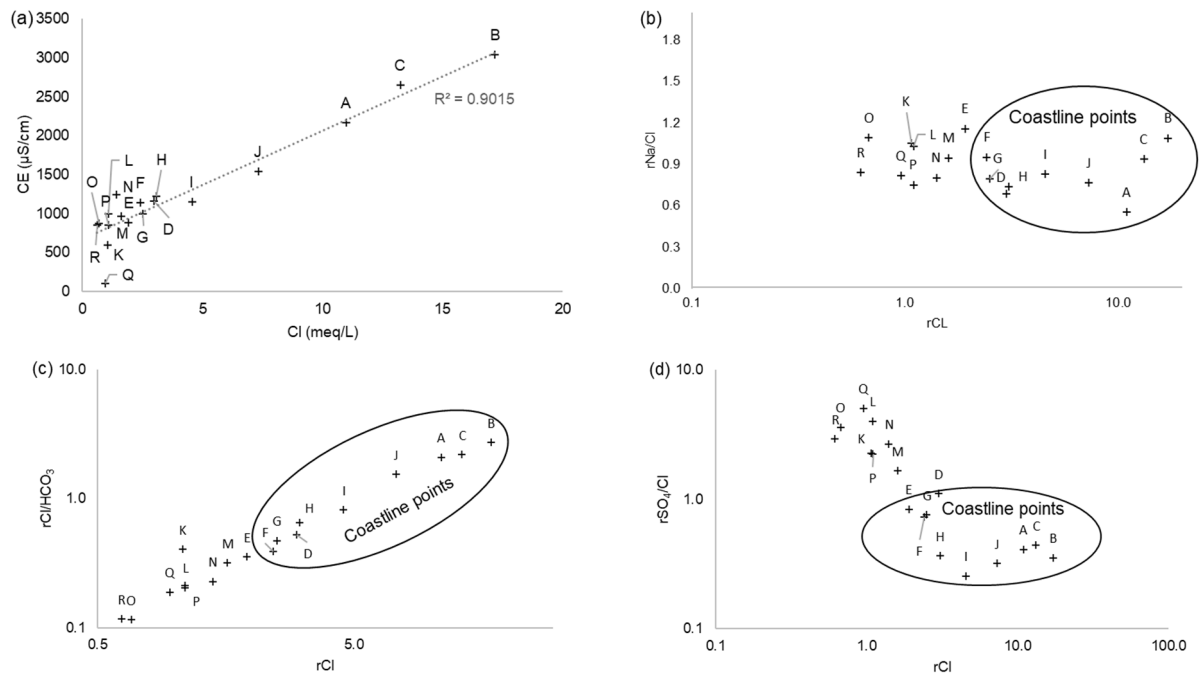
Figure 2. (**a**) Electrical conductivity vs chloride content graph; (**b**) rNaCl/rCl vs rCL chloride content graph; (**c**) rCl/rHCO$_3$ vs. rCL chloride content graph; (**d**) rSO$_4$/rCl vs. rCl graph.

The Piper, Schöeller-Berkaloff, and Stiff diagrams were used to classify and identify the main characteristics of the four types of water existing in this study zone (Figure 3).

The groundwater at control point A corresponds to a chloride-calcium (Ca-Cl) water type. Point A is monitoring the Lower Gaià waterbody and is one of the closest positions towards the SW to the coastline (0.6 km). However, it is important to highlight that hydrogeochemical point A is the only point in which a significant radical change is seen in 2020, where concentrations show a large increase of 58% in the ion HCO$_3^-$ and a decrease in the major ions Cl$^-$ (89%), NO$_3^-$ (94%), Mg^{2+} (44%), Na$^+$ (83%), and EC (50%), compared to the years 2015 to 2019, and it is classified as calcium-chloride water in 2020. This fact is probably due to the decrease in industrial and economic activities' water demands in the area during the 2020 lockdown (5,103,657 m^3 in 2020 and 6,347,000 m^3 yearly average in the 2015–2019 period [64]) and the possible reduction of saltwater intrusion in this coastal area.

The second type of water is chloride-sodic (Na-Cl), corresponding to points B (Garraf Water Body), C, and J (Lower Gaià). Points B and C are placed close to the coast (approximately 0.8 km) and J further to the SW, approximately 2.75 km from the coastal zone.

The third type of water is magnesium-bicarbonate (Mg-HCO$_3$), corresponding to Lower Gaià water body control points E, F, and K. Points E and F are located approximately to the SE, between 3 and 1 km close to the coastal zone, and K further to the SW, approximately 4.8 km away.

The fourth type of water is the calcium bicarbonate type (Ca-HCO$_3$), which comprises most of the control points (D, G, H, I, L, M, N, O, P, Q, and R) and the three water bodies defined in the area. Most of these positions (G, H, I, M, N, O, P, and R) are located in the topographically highest part of the site, starting from the NW towards the NE.
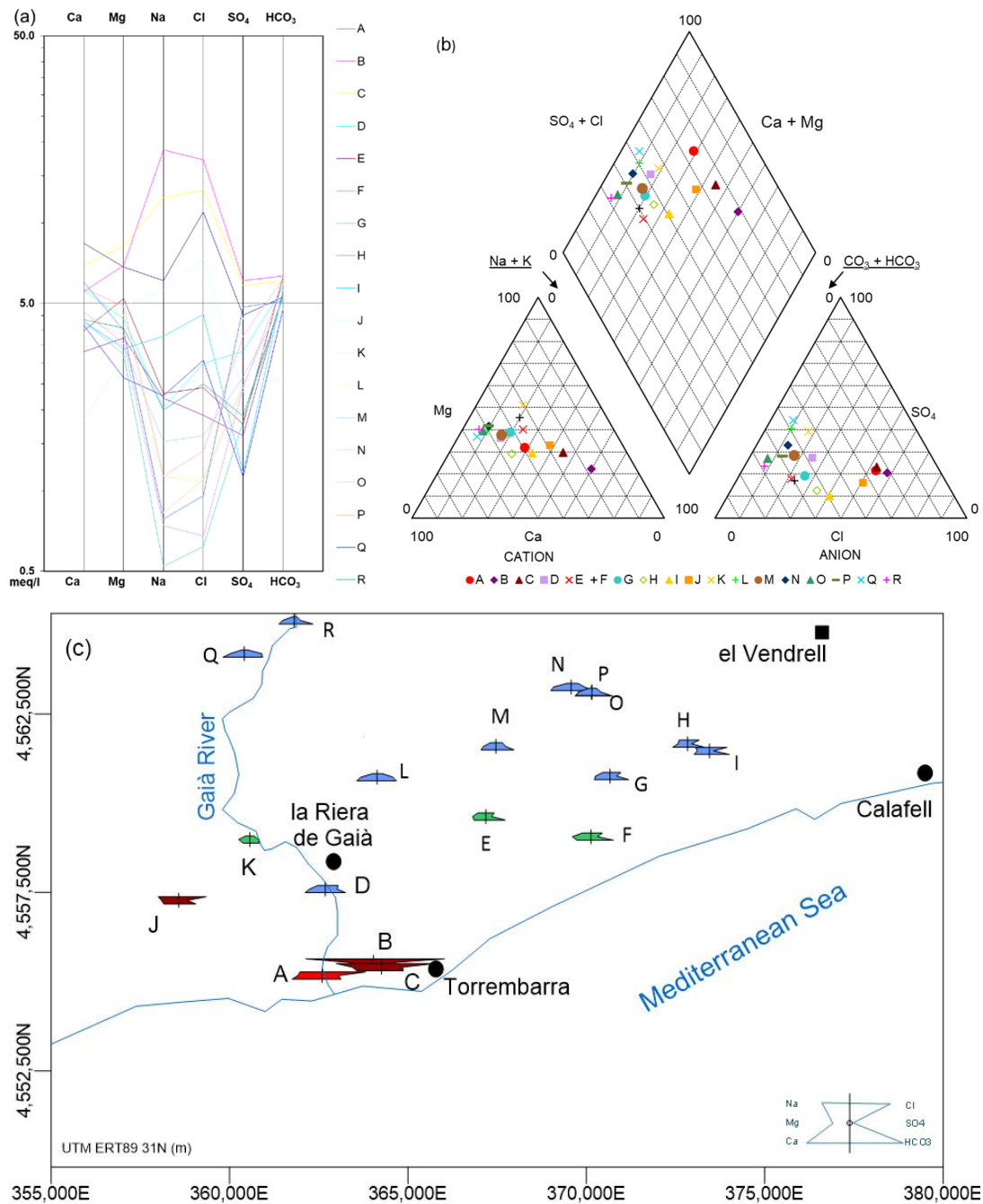
Figure 3. (**a**) Schöeller-Berkalof diagram, (**b**) Piper diagram, (**c**) Stiff Diagrams of groundwater control points at the studied site: (Ca-Cl) water types are represented in light red, (Na-Cl) types in dark red, (Mg-HCO$_3$) types in green, and (Ca-HCO$_3$) water types in blue.

4.2. Geophysical Surveys

To assess the lateral extent and thickness of the surface aquifer, geoelectrical data from 25 VES with 685 to 1000 m of survey lines was gathered within the studied zone. The VES data were acquired in 1985 by IGME using a Wenner-Schlumberger array, which is well suited to unveiling vertical geological changes [65]. Thanks to the topographic and less urbanized conditions of the terrain present in 1985, the VES acquired at that time were able to reach great extensions on the surface of the terrain on the horizontal (between 800 m and 1000 m), allowing them to also reach greater depths in the vertical (between 150 m and 200 m).

The VES results, once inverted (2.14–10.8% root mean square error), were also interpolated using IP2WIN software v3.0.1, obtaining a 2D distribution of subsurface resistivity values. We have used the lithological information available from boreholes and carried out three profile lines interpolating VES data perpendicular to the main geological structure direction to unveil the geometry of the main aquifer's units and zones with brackish/salty water (Figure 1).

The IPI2Win software v3.0.1 [57] has also been used for their representation as cross-sections.

The VES cross-sections show substantial variation in resistivity values (mainly in the 5–2000 Ω·m range). Large areas with higher resistivity values are interpreted as coarse-grained sediments and rock responses, and areas with lower resistivity values indicate the prevalence of Miocene fine-grained sediments. A general trend of decreasing electrical resistivities of the subsurface from the north to the south (coastline) has also been identified in this study area (Figure 4). The lowest resistivity values (lower than 10 Ω·m) are mainly observed in cross-section A-A' from −20 mamsl. In cross-section B, the values are found 8 m below sea level in the southern part and 120 m below sea level, 1500 m away from the coastline. The areas with electrical resistivity values below 10 Ω·m are interpreted as saturated sediments, probably with brackish/salty water, according to the coastal setting. Several authors also reported saltwater-saturated sediment responses below 10 Ω·m in different coastal settings, such as Cap-Bon, [31] Tunisia, Málaga, Spain [37], the Delta Nil Aquifer [34], and Monterrey [29].
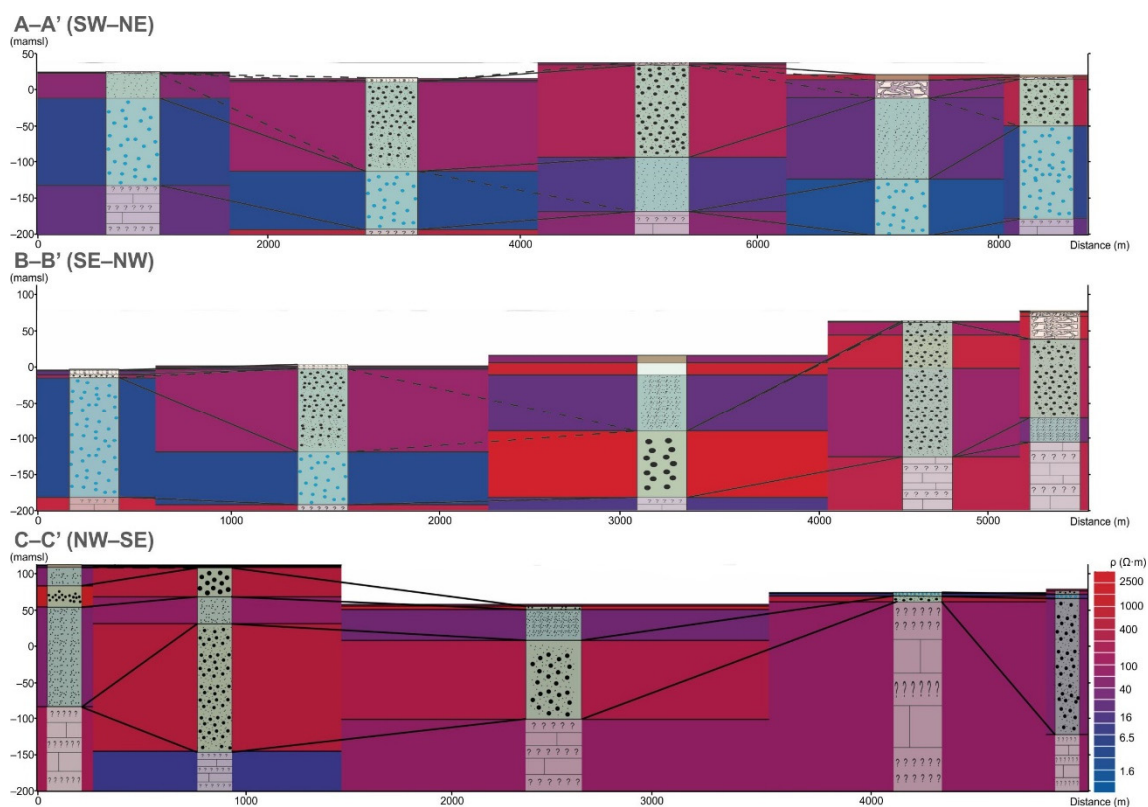

Figure 4. Electrical resistivity cross-sections and their geological interpretation were obtained from 15 VES models at the studied site. The reddish tones indicate high electrical resistivities, and the blue tones indicate lower electrical resistivities. A large dot size indicates the prevalence of Miocene coarse-grained sediments and rocks, and a low dot size indicates the prevalence of Miocene fine-grained sediments.

Moreover, we carried out a 2D ERT campaign acquiring 13 profiles—235 m in length—focused on the coastal area and the zones in which VES surveys indicated saltwater sediments (Figure 1).

We have used a mixed Wenner-Schlumberger array with 48 electrodes spaced 5 m apart for measurements. This array was chosen because it provides a moderately strong signal, is moderately sensitive to both horizontal and vertical structures [66], and provides about 40 m of maximum depth in the current research.

The ERT resistivity results (3.8–26.4% root mean square error) were also interpreted using borehole lithological information, water table measurements in piezometers, and concentrations of salinity indicators (water electrical conductivity and chloride concentration) from groundwater control points located close to the Torrembarra and Altafulla sites (Figures 5 and 6).
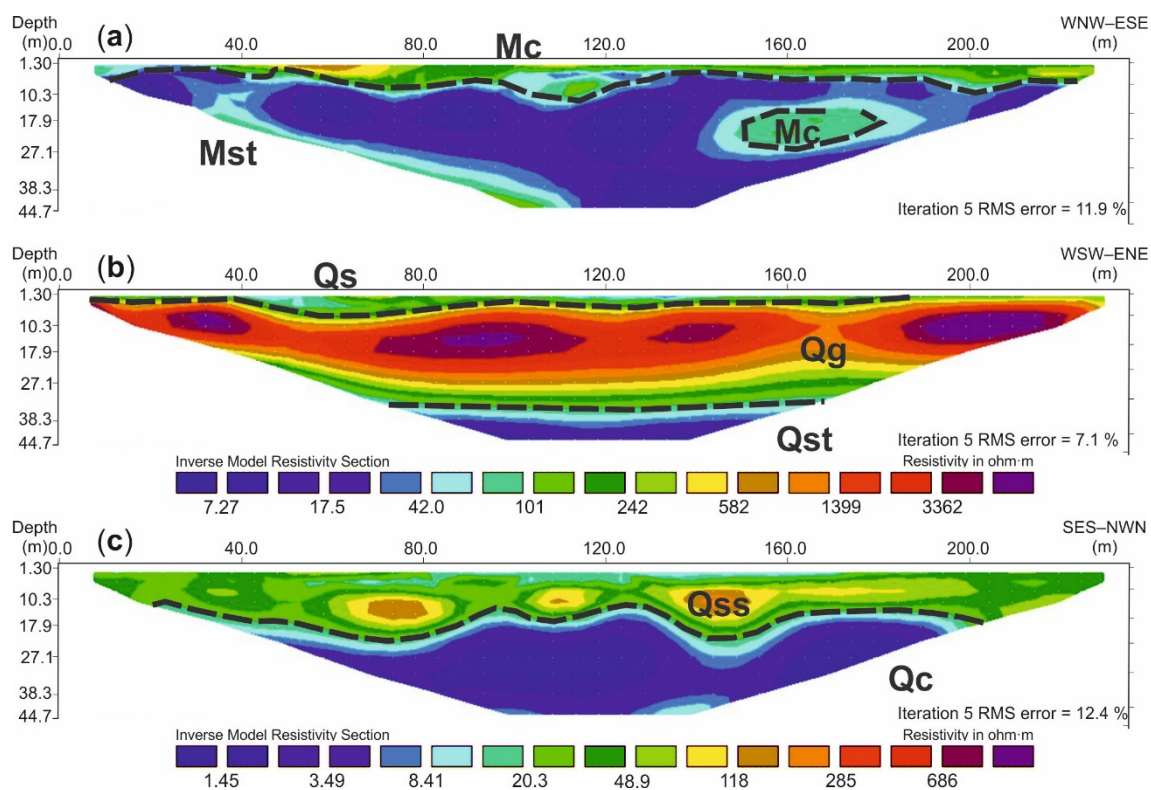

Figure 5. (**a**) Interpreted ERT cross-section 2 over consolidated sediments and rocks. Mc: Miocene sand and calcarenite, Ms: Miocene silt, (**b**) Interpreted ERT cross-section 5 over unconsolidated sediments. Qs: Quaternary sand, Qg: Quaternary gravel and sand, Qst: Quaternary silt, (**c**) Interpreted ERT cross-section 7 close to Torrembarra coastline. Qss: Quaternary sand and silt, Qc: Quaternary clay.

We have acquired the ERT cross-sections over mainly consolidated sediments (1, 2, 3, 9, and 10), within quaternary sediments (4, 5, 6, 11, 12, and 13), and close to the coastline (7 and 8) (see ERT locations in Figure 6).

In profiles acquired over consolidated sediments, two geoelectric units can be identified (Figure 5). The shallowest layer is characterized by 200–1500 $\Omega \cdot$m values and could be identified at the upper part of the geoelectrical cross-sections. The layer has an average thickness of 10 m and is interpreted as unsaturated Miocene-age sandstones and calcarenites.

Underneath, the ERT geoelectrical cross-sections show a single layer with variable and fluctuating thickness that is defined by values less than 100 $\Omega \cdot$m. The resistivity values are interpreted as Micoene siltstone and saturated Miocene sedimentary rock responses. The

water level is interpreted in these sections from 10 m depth (ERT cross-section 10) to 35 m depth (ERT cross-section 3).
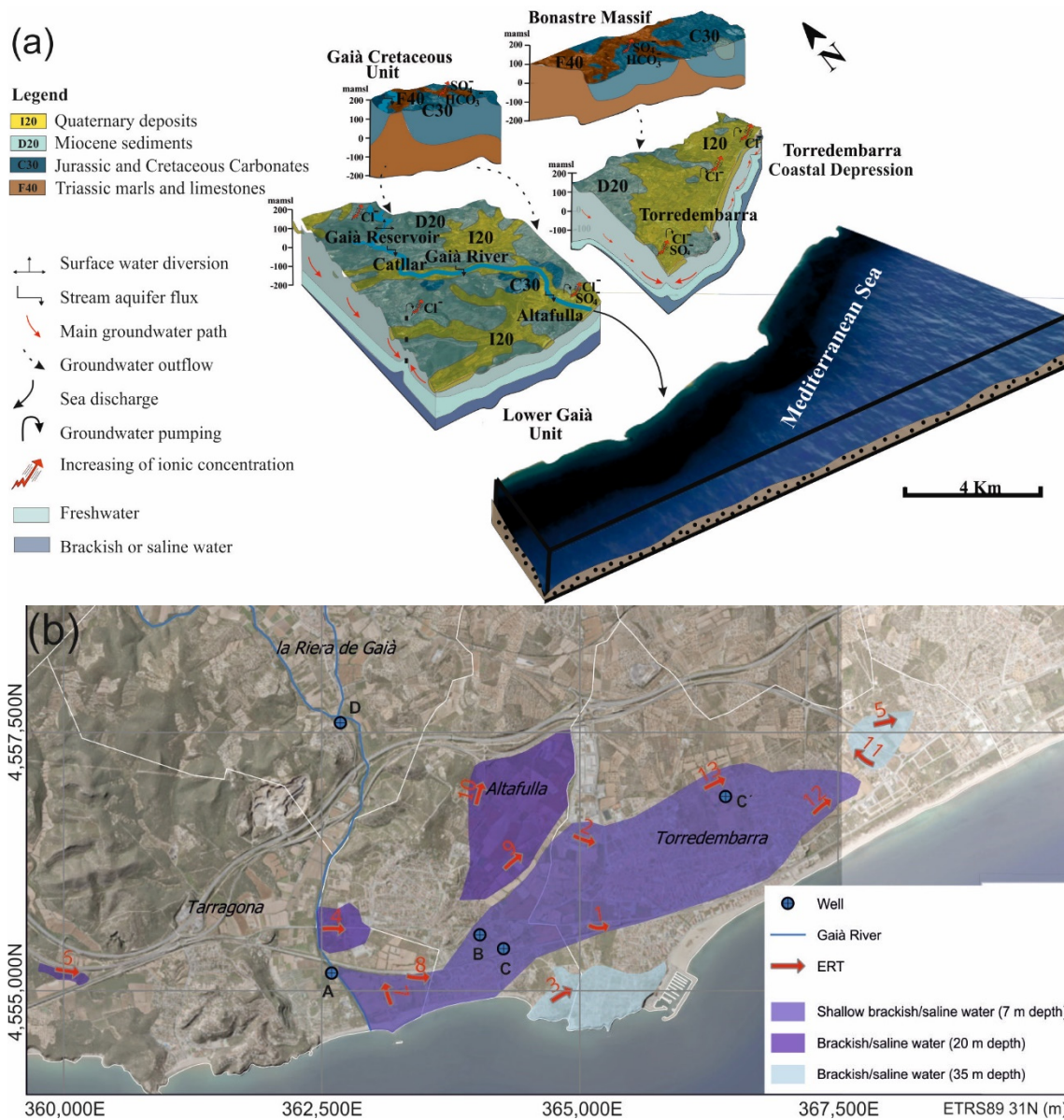
Figure 6. (**a**) Bonastre-Torredembarra hydrogeological model; (**b**) Altafulla-Torredembarra groundwater salinity map inferred from ERT results, topography, and hydrogeochemical parameters from nearby groundwater control points.

In profiles acquired over unconsolidated/slightly consolidated sediments, three geoelectric units can be identified:

- 500–1000 $\Omega \cdot$m layer interpreted as gravels and/or carbonate rocks (Upper Pleistocene).
- 5–50 $\Omega \cdot$m levels corresponding to clay and silt responses (Upper Pleistocene).
- 100–200 $\Omega \cdot$m interpreted as sand and gravel (Holocene–Upper Pleistocene).

In profiles acquired close to sea level, the electrical values are generally lower than 300 $\Omega \cdot$m, and two geoelectric units can be identified. The upper layer is characterized by values from 20–500 $\Omega \cdot$m, has a thickness of 7–25 m, and is interpreted as sandy and silty sediments.

Below, the ERT geoelectrical cross-sections show a single layer with variable thickness that is distinguished by values lower than 20 Ω·m. These figures are interpreted as clay and silt responses and/or brackish/salty saturated sediments (Holocene).

4.3. Hydrogeological Conceptual Model and Groundwater Salinization Map

From the joint interpretation of all the data and results, a hydrogeological conceptual model and a groundwater salinization map have been made (Figure 6). The underground flows that recharge the system come from the upper part, upstream of the Gaià Reservoir and part of the Gaia Cretaceous unit, while in the eastern sector, the waters coming from the southern pre-litoral unit and south pre-coastal unit feed the coastal aquifer system of the Torredembarra area.

A large part of the aquifer system drains towards the sea, except for the el Catllar town sector, where the flows drain towards the east, which corresponds to the Tarragona city coastal unit.

Concerning anthropic interventions, a significant volume is extracted from the pumping wells, mainly for agricultural and industrial use, and according to the background hydrochemical data and the data presented in Section 4.1, there is evidence of a decrease in the marine intrusion effect on the water quality of the Torredembarra-Altafulla coastal aquifer system. The effect of the marine intrusion as described by [39,67] on the sector has receded, with a general decrease in the parameters of electrical conductivity, chlorides, and sulfates. This, to the extent that the origin of the sulfate comes not only from marine intrusion but also from the groundwater recharge water upstream, has a significant and important mark.

Nevertheless, it is important to highlight that some marine intrusion effects remain, and we have performed a groundwater salinization map based on ERT, topography, and hydrochemical data of the Torredembara-Altafulla zone. The map divides the studied area into four groups:

- High-depth groundwater salinity. ERT cross sections show lower base resistivity values, which could indicate water with a high salt concentration.
- Medium-depth groundwater salinity. ERT cross sections show values related to brackish and/or saline water responses not exceeding 20 m depth.
- Low-depth groundwater salinity. Saltwater intrusion is present in most of the cross-section and is located at a depth of approximately 7 m.

5. Conclusions

We have carried out a regional-to-local-scale quantitative and qualitative study of the aquifer system to define a hydrogeological conceptual model of the coastal aquifer, characterize the hydrogeochemistry of groundwater, and identify the areas prone to being affected by the saline intrusion in the Torredembarra-Altafulla zone. The use of VES surveys enables a regional characterization of the aquifer system and the zones with the potential to be affected by saltwater intrusion, while ERT surveys are well suited to provide a highly detailed characterization of the coastal aquifer and delimit the zone both in extension and depth.

The obtained results could be used as a support tool for the evaluation of the most favorable areas for groundwater withdrawal, as well as enabling the protection and control of the most susceptible areas to be polluted by saltwater intrusion. Anyway, the use of indirect geophysical methods will limit the number of new piezometers for improving the groundwater model and the subsequent risk of coming into contact with different water bodies during drilling operations.

Author Contributions: Conceptualization, A.C.; methodology, A.S., A.C., M.H. and I.J.C.; formal analysis, A.S. and A.C.; data curation, I.J.C., A.U., A.S. and R.L.; writing—original draft preparation, A.S.; writing—review and editing, I.J.C., A.U., R.L., L.R., M.H., J.C.T., A.C., R.G.-A. and A.S. All authors have read and agreed to the published version of the manuscript.

References

1. Van der Gun, J. *Groundwater and Global Change: Trends, Opportunities and Challenges | International Groundwater Resources Assessment Centre*; United Nations Educational, Scientific and Cultural Organization: Paris, France, 2012; ISBN 9789230010492.
2. Aeschbach-Hertig, W.; Gleeson, T. Regional strategies for the accelerating global problem of groundwater depletion. *Nat. Geosci.* **2012**, *5*, 853–861. [CrossRef]
3. Akbarpour, S.; Niksokhan, M.H. Investigating effects of climate change, urbanization, and sea level changes on groundwater resources in a coastal aquifer: An integrated assessment. *Environ. Monit. Assess.* **2018**, *190*, 579. [CrossRef] [PubMed]
4. Fetter, C.W. *Applied Hydrogeology*, 4th ed.; Prentice Hal: Upper Saddle River, NJ, USA, 2001; ISBN 0-13-088239-9.
5. López-Geta, J.A.; de la Orden, J.A.; Gómez, J.D.; Ramos, G.; Mejías, M.; Rodriguez, L. *Coastal Aquifers Intrusion Technology: Mediterranean Countries*; Instituto Geológico y Minero de España: Madrid, Spain, 2003; ISBN 84-7840-469-4.
6. Mastrocicco, M.; Colombani, N. The Issue of Groundwater Salinization in Coastal Areas of the Mediterranean Region: A Review. *Water* **2021**, *13*, 90. [CrossRef]
7. Custodio Gimena, E. *Evaluación de la Gestión y Gobernanza del Agua Subterránea: Aplicación a Áreas Seleccionadas Españolas: (EGASE)*; Universidad Politécnica de Cataluña: Barcelona, Spain, 2022; ISBN 9788498804324.
8. Polemio, M.; Zuffiano, M. Review of Utilization Management of Groundwater at Risk of Salinization. *J. Water Resour. Plan. Manag.* **2020**, *146*, 3120002. [CrossRef]
9. Losada, I.J.; Izaguirre, C.; Díaz, P. *Cambio Climático en la Costa Española*; Ministerio de Agricultura, Alimentación y Medio Ambiente, Gobierno de España: Madrid, Spain, 2014; ISBN 978-84-491-1403-8.
10. Alfarrah, N.; Walraevens, K. Groundwater overexploitation and seawater intrusion in coastal areas of arid and semi-arid regions. *Water* **2018**, *10*, 143. [CrossRef]
11. Alexander, L.; Allen, S.; Bindoff, N.; Breon, F.-M.; Church, J.; Cubasch, U.; Emori, S.; Forster, P.; Friedlingstein, P.; Gillett, N.; et al. Climate change 2013: The physical science basis, in contribution of Working Group I (WGI) to the Fifth Assessment Report (AR5) of the Intergovernmental Panel on Climate Change (IPCC). In *Climate Change 2013: The Physical Science Basis*; Cambridge University Press: Cambridge, UK, 2013.
12. Post, V.E.A. Fresh and saline groundwater interaction in coastal aquifers: Is our technology ready for the problems ahead? *Hydrogeol. J.* **2005**, *13*, 120–123. [CrossRef]
13. UNESCO. Framework for groundwater monitoring in (semi-)arid regions. In *Studies in Hydrology 92-3-103679-7*; Van Lanen, H., Carrillo-Rivera, J., Eds.; Paris, France, 1998; Volume 57, pp. 7–20, ISBN 92-3-103679-7.
14. UNESCO. *Submarine Groundwater Discharge: Management Implications, Measurements and Effects. Groundwater Series n. 5.*; IHP: Paris, France, 2004; ISBN 92-9220-006-2.
15. Margat, J.; van der Gun, J. *Groundwater around the World: A Geographic Synopsis*; CRC Press Taylor & Francis Group: Boca Raton, FL, USA, 2013; ISBN 978-1-138-00034-6.
16. Sabater, S.; Barceló, D. *Water Scarcity in the Mediterranean: Perspectives under Global Change*; Springer: Berlin, Germany, 2010; ISBN 978-3-642-03970-6(H).
17. López-Geta, J.A. La gestión de los acuíferos costeros como fuente de un recurso importante y estratégico. progreso y futuro; In *Las Aguas Subterráneas en la Ley de Aguas Española: Un Decenio de Experiencia*; AIH: Madrid, Spain, 1995; pp. 221–237.
18. Custodio, E. Coastal aquifers of Europe: An overview. *Hydrogeol. J.* **2010**, *18*, 269–280. [CrossRef]
19. ACA. *Memòria Tècnica del Programa de Seguiment i Control (PSiC) del Districte de Conca Fluvial de Catalunya. Període 2019–2024*; Agència Catalana de l'Aigua: Barcelona, Spain, 2019.
20. Lekula, M.; Lubczynski, M.W.; Shemang, E.M. Hydrogeological conceptual model of large and complex sedimentary aquifer systems—Central Kalahari Basin. *Phys. Chem. Earth, Parts A/B/C* **2018**, *106*, 47–62. [CrossRef]
21. Binley, A.; Hubbard, S.S.; Huisman, J.A.; Revil, A.; Robinson, D.A.; Singha, K.; Slater, L.D. The emergence of hydrogeophysics for improved understanding of subsurface processes over multiple scales. *Water Resour. Res.* **2015**, *51*, 3837–3866. [CrossRef]
22. Goldman, M.; Kafri, U. Hydrogeophysical applications in coastal aquifers. In *Applied Hydrogeophysics*; Vereecken, H., Binley, A., Cassiani, G., Revil, A., Titov, K., Eds.; Springer: Dordrecht, The Netherlands, 2006; pp. 233–254.
23. Werner, A.D.; Bakker, M.; Post, V.E.A.; Vandenbohede, A.; Lu, C.; Ataie-Ashtiani, B.; Simmons, C.T.; Barry, D.A. Seawater intrusion processes, investigation and management: Recent advances and future challenges. *Adv. Water Resour.* **2013**, *51*, 3–26. [CrossRef]

24. Benabdelouahab, S.; Salhi, A.; Himi, M.; Stitou El Messari, J.E.; Casas Ponsati, A. Geoelectrical investigations for aquifer characterization and geoenvironmental assessment in northern Morocco. *Environ. Earth Sci.* **2019**, *78*, 209. [CrossRef]

25. Vann, S.; Puttiwongrak, A.; Suteerasak, T.; Koedsin, W. Delineation of seawater intrusion using geo-electrical survey in a coastal aquifer of Kamala beach, Phuket, Thailand. *Water* **2020**, *12*, 506. [CrossRef]

26. Koefoed, O. *Geosounding Principles 1: Resistivity Sounding Measurements*; Elsevier Science Publishing Company: Amsterdam, The Netherlands, 1979.

27. Cimino, A.; Cosentino, C.; Oieni, A.; Tranchina, L. A geophysical and geochemical approach for seawater intrusion assessment in the Acquedolci coastal aquifer (Northern Sicily). *Environ. Geol.* **2008**, *55*, 1473–1482. [CrossRef]

28. Paz, M.C.; Alcalá, F.J.; Medeiros, A.; Martínez-Pagán, P.; Pérez-Cuevas, J.; Ribeiro, L. Integrated MASW and ERT imaging for geological definition of an unconfined alluvial aquifer sustaining a coastal groundwater-dependent ecosystem in southwest Portugal. *Appl. Sci.* **2020**, *10*, 5905. [CrossRef]

29. Goebel, M.; Pidlisecky, A.; Knight, R. Resistivity imaging reveals complex pattern of saltwater intrusion along Monterey coast. *J. Hydrol.* **2017**, *551*, 746–755. [CrossRef]

30. Hasan, M.; Shang, Y.; Jin, W.; Shao, P.; Yi, X.; Akhter, G. Geophysical Assessment of Seawater Intrusion into Coastal Aquifers of Bela Plain, Pakistan. *Water* **2020**, *12*, 3408. [CrossRef]

31. Kouzana, L.; Benassi, R.; Ben mammou, A.; Sfar felfoul, M. Geophysical and hydrochemical study of the seawater intrusion in Mediterranean semi arid zones. Case of the Korba coastal aquifer (Cap-Bon, Tunisia). *J. Afr. Earth Sci.* **2010**, *58*, 242–254. [CrossRef]

32. Cosentino, P.; Capizzi, P.; Fiandaca, G.; Martorana, R.; Messina, P.; Pellerito, S. Study And Monitoring Of Salt Water Intrusion In The Coastal Area Between Mazara Del Vallo And Marsala (South-Western Sicily). In *Methods and Tools for Drought Analysis and Management*; Rossi, G., Vega, T., Bonaccorso, B., Eds.; Springer: Dordrecht, The Netherlands, 2007; pp. 303–321, ISBN 978-1-4020-5924-7.

33. El Osta, M.; Masoud, M.; Badran, O. Aquifer hydraulic parameters estimation based on hydrogeophysical methods in West Nile Delta, Egypt. *Environ. Earth Sci.* **2021**, *80*, 344. [CrossRef]

34. Abu Salem, H.S.; Gemail, K.S.; Junakova, N.; Ibrahim, A.; Nosair, A.M. An Integrated Approach for Deciphering Hydrogeochemical Processes during Seawater Intrusion in Coastal Aquifers. *Water* **2022**, *14*, 1165. [CrossRef]

35. Galazoulas, E.C.; Mertzanides, Y.C.; Petalas, C.P.; Kargiotis, E.K. Large Scale Electrical Resistivity Tomography Survey Correlated to Hydrogeological Data for Mapping Groundwater Salinization: A Case Study from a Multilayered Coastal Aquifer in Rhodope, Northeastern Greece. *Environ. Process.* **2015**, *2*, 19–35. [CrossRef]

36. Sendrós, A.; Urruela, A.; Himi, M.; Alonso, C.; Tapias, J.C.; Rivero, L.; Garcia-Artigas, R.; Casas, A. Characterization of a Shallow Coastal Aquifer in the Framework of a Subsurface Storage and Soil Aquifer Treatment Project Using Electrical Resistivity Tomography (Port de la). *Appl. Sci.* **2021**, *11*, 2448. [CrossRef]

37. Martínez, J.; Benavente, J.; García-Aróstegui, J.L.; Hidalgo, M.C.; Rey, J. Contribution of electrical resistivity tomography to the study of detrital aquifers affected by seawater intrusion-extrusion effects: The river Vélez delta (Vélez-Málaga, southern Spain). *Eng. Geol.* **2009**, *108*, 161–168. [CrossRef]

38. ICGC. *Tarragonès - Mapa Geològic Comarcal de Catalunya - 1:50000*; Institut Cartogràfic i Geològic de Catalunya: Barcelona, Spain, 2005.

39. FCIHS. *Estudio Hidrogeológico del Bajo Gaià Desde el Embalse del Catllar Hasta el Mar (Tarragonès, Tarragona)*; 46 Curso Internacional de Hidrología Subterránea: Barcelona, Spain, 2012.

40. IGME. *Estudio de Los Recursos Hídricos Subterráneos del Sistema Hidrogeológico 74. Camp de Tarragona*, 1st ed.; Instituto Geológico y Minero de España: Madrid, Spain, 1986; ISBN 84-7474-347-8.

41. AEMet. *Guía Resumida del Clima en España (1981–2010)*; Ministerio de Agricultura, Alimentación y Medio Ambiente; Gobierno de España: Madrid, Spain, 2012.

42. ACA. Catalonia Water Quality Control Data. Agència Catalana de l'Aigua. Departament de Territori i Sosteniblitat. Generalitat de Catalunya. Available online: http://aca-web.gencat.cat/sdim21/ (accessed on 2 November 2021).

43. Sanz, J.; Suescun, J.; Molist, J.; Rubio, F.; Mujeriego, R.; Salgado, B. Reclaimed water for the Tarragona petrochemical park. *Water Supply* **2014**, *15*, 308–316. [CrossRef]

44. IDESCAT. *Estimacions Població Estacional Torredembarra-Altafulla 2016*; Institut d'Estadística de Catalunya; Generalitat de Catalunya: Barcelona, Spain, 2022.

45. Cabrera, L.; Calvet, F. Onshore Neogene record in NE Spain: Vallès–Penedès and El Camp half-grabens (NW Mediterranean). In *Tertiary Basins of Spain: The Stratigraphic Record of Crustal Kinematics*; Friend, P.F., Dabrio, C.J.E., Eds.; World and Regional Geology; Cambridge University Press: Cambridge, UK, 1996; pp. 97–105.

46. SGE. *Geología de España*; Vera, J.A., Ed.; Instituto Geológico y Minero de España: Madrid, Spain, 2004; ISBN 84-7840-546-1.

47. IGME. *Mapa Hidrogeológico de España. E 1:50.000. Tarragona*; Instituto Geológico y Minero de España: Madrid, Spain, 1989.

48. *ISO/IEC 17020:2012*; Conformity Assessment. Requirements for the Operation of Various Types of Bodies Performing Inspection. Asociación Española de Normalización y Certificación: Madrid, Spain, 2012.

49. APHA. *Standard Methods for the Examination of Water and Wastewater*; American Public Health Association: Washington, DC, USA, 2012; Volume 10.

50. Vazquéz-Suñe, E.; Serrano-Juan, A. *EasyQuim*; Institute of Environmental Assessment and Water Research: Barcelona, Spain, 2012.

51. Piper, A.M. A graphic procedure in the geochemical interpretation of water-analyses. *Eos Trans. Am. Geophys. Union* **1944**, *25*, 914–928. [CrossRef]

52. Schoeller, H. Qualitative Evaluation of Ground Water Resources. In *Water Resource Series No. 33*; UNESCO: Paris, France, 1967; pp. 44–52.

53. Custodio, E.; Llamas, M.R. *Hidrología Subterránea*, 2nd ed.; Omega: Barcelona, Spain, 2001; Volume I, ISBN 978-84-282-0447-7.

54. Sendrós, A.; Díaz, Y.; Himi, M.; Tapias, J.C.; Rivero, L.; Font, X.; Casas, A. An evaluation of aquifer vulnerability in two nitrate sensitive areas of Catalonia (NE Spain) based on electrical resistivity methods. *Environ. Earth Sci.* **2014**, *71*, 77–84. [CrossRef]

55. Casas, A.; Himi, M.; Díaz, Y.; Pinto, V.; Font, X.; Tapias, J.C. Assessing aquifer vulnerability to pollutants by electrical resistivity tomography (ERT) at a nitrate vulnerable zone in NE Spain. *Environ. Geol.* **2008**, *54*, 515–520. [CrossRef]

56. Dahlin, T. 2D resistivity surveying for environmental and engineering applications. *First Break* **1996**, *14*, 275–284. [CrossRef]

57. Bovachev, A.A.; Modin, I.N.; Shevnin, V.A. 1D Interpretation of VES profile (IPI2Win). 2011, Volume 33. Available online: http://geophys01.geol.msu.ru/ipi2win.htm (accessed on 2 November 2021).

58. Loke, M.H.; Dahlin, T. A comparison of the Gauss–Newton and quasi-Newton methods in resistivity imaging inversion. *J. Appl. Geophys.* **2002**, *49*, 149–162. [CrossRef]

59. Loke, M.H.; Barker, R.D. Rapid least-squares inversion of apparent resistivity pseudosections by a quasi-Newton method. *Geophys. Prospect.* **1996**, *44*, 131–152. [CrossRef]

60. ACA. *Avaluació de la Problemàtica Originada Per L'excés de Nitrats D'origen Agrari en Les Masses D'aigua Subterrània a Catalunya: Informe Tècnic*; Agència Catalana de l'Aigua: Barcelona, Spain, 2016.

61. El Osta, M.; Masoud, M.; Alqarawy, A.; Elsayed, S.; Gad, M. Groundwater Suitability for Drinking and Irrigation Using Water Quality Indices and Multivariate Modeling in Makkah Al-Mukarramah Province, Saudi Arabia. *Water* **2022**, *14*, 483. [CrossRef]

62. Setiawan, I.; Morgan, L.; Doscher, C.; Ng, K.; Bosserelle, A. Mapping shallow groundwater salinity in a coastal urban setting to assess exposure of municipal assets. *J. Hydrol. Reg. Stud.* **2022**, *40*, 100999. [CrossRef]

63. Fontalva, J.M.G.; Calvache, M.L.; Duque, C. Origen de la salinidad de las aguas subterráneas del sistema acuífero costero de Torrevieja: Aspectos Hidroquímicos. *Geogaceta* **2010**, *48*, 127–130.

64. ACA. *Agència Catalana de l'aigua, Consumption and Volume Studies*; Agència Catalana de l'Aigua: Barcelona, Spain, 2021.

65. Dahlin, T.; Zhou, B. A numerical comparison of 2D resistivity imaging with 10 electrode arrays. *Geophys. Prospect.* **2004**, *52*, 379–398. [CrossRef]

66. Martorana, R.; Fiandaca, G.; Casas Ponsati, A.; Cosentino, P.L. Comparative tests on different multi-electrode arrays using models in near-surface geophysics. *J. Geophys. Eng.* **2009**, *6*, 1–20. [CrossRef]

67. Puigserver, D.; Carulla, N.; Torras, B.; Iglesias, M.; Pérez, A.; Borrás, X.; Carmona, J. Hydrogeological Recovery of the Over-exploited Baix Francoli-Gaia Block Aquifer System (Spain). In *Groundwater-Present Status and Future Task, Proceedings of the 34th Congress of International Association of Hydrogeologists, Beijing, China, 9 September 2006*; The International Association of Hydrogeologists: Beijing, China, 2006.